NUMERICAL MODELLING OF TSUNAMIS GENERATED BY GRANULAR LANDSLIDES IN OPENFOAM®

Romano A[1],[2] Lara J[3], Barajas G[4], Losada IJ[5]

Landslide-generated tsunamis are a relevant source of hazard for coastal areas. In this paper, the preliminary modelling results of tsunamis generated by deformable landslides by using computational fluid dynamics (CFD) methods, in OpenFOAM®, is presented. The numerical approach presented here consists in modelling the granular material by using a Coulomb viscoplastic rheology. This numerical model is applied to reproduce three literature benchmark cases (2D submerged, 2D and 3D subaerial, respectively). Some preliminary qualitative and quantitative numerical results, compared to the experimental ones, are presented in the paper.

Keywords: Tsunamis; Granular Landslides; Numerical Modelling

INTRODUCTION

Impulsive waves (i.e., tsunamis) can be generated by sudden displacements of volumes of water induced by earthquakes, landslides, volcanic eruptions, impacts of asteroids and gradients of atmospheric pressure (Løvholt et al., 2015). Among these triggering mechanisms, landslides assume a relevant role, especially as far as confined geometries are concerned (e.g. bays, reservoirs, lakes, islands, fjords, etc.).

Several devastating landslide tsunami events occurred in the past. It is worth citing the event occurred in 1958 at Lituya Bay (Alaska, Fritz et al., 2009) that caused the largest wave runup ever recorded in modern times (almost 525 m) killing 5 people, the Vajont Valley event (Italy, Panizzo et al., 2005) in 1963, that destroyed 4 villages causing the loss of nearly 2,000 human lives and severe socio-economic consequences. More recently, the Anak Krakatoa event (Indonesia, Grilli et al., 2019) in 2018, when the volcano flank collapse triggered a tsunami that caused several hundreds of casualties.

The physical process are generally characterized by smaller length and time scales than those of tsunamis generated by earthquakes. When the landslide occurs directly at the water body boundaries, impulsive waves both radiate seaward and propagate alongshore. Since the tsunamis generation is likely to occur in shallow water regions, the interaction between the waves and the sloping sea bottom plays immediately a relevant role. The waves can be refracted by the interaction with the bottom, and trapping mechanisms, like those typical of edge waves, can occur (Romano et al., 2013; Bellotti and Romano, 2017). The complex interaction that exists between the generation and the propagation mechanisms needs to be carefully considered for a proper understanding of the generated waves features and, consequently, for developing effective Tsunamis Early Warning Systems (TEWS) that works in real-time (Cecioni et al., 2011; De Girolamo et al., 2014) and Probabilistic Tsunamis Hazard Assessment (PTHA) tools (Grilli et al., 2009).

Landslide tsunamis have been studied by means of physical, numerical and analytical models. Different approaches have been used for physical modelling of such a phenomenon, considering both rigid (Watts, 1998; Liu et al., 2005; Enet and Grilli, 2007; Di Risio et al., 2009a,b; Romano et al., 2013, 2016, 2017; Heller and Spinneken, 2015) and deformable/granular (Heller and Hager, 2010; Mohammed and Fritz, 2012; Viroulet et al., 2014; Lindstrøm, 2016; McFall and Fritz, 2016; Zitti et al., 2016; Grilli et al., 2017; Takabatake et al., 2022) landslides in 2D and 3D configurations. Similarly, as far as numerical models are considered, several approaches have been used for modelling landslide tsunamis, employing both depth-averaged models, using Non-Linear Shallow Water or Boussinesq Equations (e.g. Watts et al., 2003; Lynett and Liu, 2005; Liu et al., 2005; Løvholt et al., 2005; Bellotti et al., 2008; Cecioni et al., 2011; Grilli et al., 2017; Si et al., 2018; Kim et al., 2019b; Ruffini et al., 2019; Grilli et al., 2019) and/or computational fluid dynamics (CFD) methods that allows to model in detail the complex phenomena that take place during the

[1]Roma Tre University, Engineering Department, Rome, Italy, alessandro.romano@uniroma3.it
[2]IHCantabria - Instituto de Hidráulica Ambiental de la Universidad de Cantabria, Santander, Spain
[3]IHCantabria - Instituto de Hidráulica Ambiental de la Universidad de Cantabria, Santander, Spain
[4]IHCantabria - Instituto de Hidráulica Ambiental de la Universidad de Cantabria, Santander, Spain
[5]IHCantabria - Instituto de Hidráulica Ambiental de la Universidad de Cantabria, Santander, Spain

generation and near-field propagation phases. Different CFD numerical methods used to simulate landslide-generated tsunamis, modelling the landslide body as a rigid impermeable model (e.g. Montagna et al., 2011; Whittaker et al., 2017; Kim et al., 2019a; Chen et al., 2020; Romano et al., 2020) or as a deformable/granular material Løvholt et al. (2005); Abadie et al. (2010); Ma et al. (2015); Heller et al. (2016); Shi et al. (2016); Kim et al. (2019b); Si et al. (2018); Clous and Abadie (2019); Mulligan et al. (2020); Franci et al. (2020); Paris et al. (2021); Rauter et al. (2021, 2022); Lee and Huang (2022), modelling also real cases (La Palma, Canary Island, Abadie et al., 2012, 2019), Anak Krakatau (Indonesia, Grilli et al., 2019), and Lake Askja (Iceland, Rauter et al., 2022).

In this paper, the preliminary modelling results of tsunamis generated by deformable landslides by using CFD methods, in OpenFOAM®, is presented. The numerical approach presented here consists in modelling the granular material by using a Coulomb viscoplastic rheology (Non-Newtonian rheology, Domnik and Pudasaini, 2012; von Boetticher et al., 2016) implemented in *multiPhaseInterFoam* (OpenFOAM-v2106 standard solver, for multiple incompressible fluids which captures the interfaces and includes surface-tension and contact-angle effects for each phase). This numerical framework is applied to reproduce three literature benchmark cases identified by tsunamis experts: I) a 2D submerged landslide case (Grilli et al., 2017); II) a 2D subaerial landslide case (Viroulet et al., 2014); III) a 3D subaerial landslide case (Mohammed and Fritz, 2012).

The paper is structured as follows. After this introduction, the description of the numerical model framework (i.e., OpenFOAM®)is provided. Then, a brief description of the landslide-generated tsunamis expertimental benchmark cases is given. The preliminary numerical results are then presented and, finally, a concluding remarks section closes the paper.

NUMERICAL MODEL

The numerical modelling of tsunamis generated by deformable landslides, described in this paper, has been developed on the OpenFOAM® platform (Jasak, 1996). IHFOAM (Higuera et al., 2013a,b), based on interFoam of OpenFOAM®, includes wave boundary conditions and porous media solvers (Romano et al., 2020) for coastal and offshore engineering applications and can solve both three dimensional Reynolds-Averaged Navier-Stokes equations (RANS) and Volume-Averaged Reynolds-Averaged Navier-Stokes equations (VARANS) for two phase flows. RANS and VARANS equations are solved coupled to the Volume of Fluid (VOF) equation. In this section the base equations as well as a description of the proposed method are presented.

Governing equations

The RANS equations, used to model the flow at the clear fluid region, are based on the Reynolds decomposition, that identifies an average and a fluctuating component (i.e. velocity and pressure fields for incompressible models). These equations are represented by the mass and momentum conservation equations, coupled to the VOF equation as follows:

$$\frac{\partial u_i}{\partial x_i} = 0 \tag{1}$$

$$\frac{\partial \rho u_i}{\partial t} + u_j \frac{\partial \rho u_i}{\partial x_j} = -g_j x_j \frac{\partial \rho}{\partial x_i} - \frac{\partial p^*}{\partial x_i} - f_{\sigma i} - \frac{\partial}{\partial x_j} \mu_{\text{eff}} \left(\frac{\partial \rho u_i}{\partial x_j} + \frac{\partial \rho u_j}{\partial x_i} \right) \tag{2}$$

$$\frac{\partial \alpha}{\partial t} + \frac{\partial u_i \alpha}{\partial x_i} + \frac{\partial u_{ci} \alpha (1-\alpha)}{\partial x_i} = 0 \tag{3}$$

where u_i (m/s) are the ensemble averaged components of the velocity, x_i (m) the Cartesian coordinates, g_j (m/s^2) the components of the gravitational acceleration, ρ (kg/m^3) the density of the fluid, p^* the ensemble averaged pressure in excess of hydrostatic, defined as $p^* = p - \rho g_j x_j$ (Pa), being p the total pressure, α (-) the volume fraction (VOF indicator function) which is assumed to be 1 for the water phase and 0 for the air phase, $f_{\sigma i}$ (N/m^3) the surface tension, defined as $f_{\sigma i} = \sigma \kappa \frac{\partial \alpha}{\partial x_i}$, where σ (N/m) is the surface tension constant and κ (1/m) the curvature (Brackbill et al., 1992). μ_{eff} (Pa $\cdot$ s) is the effective dynamic viscosity that is defined as $\mu_{\text{eff}} = \mu + \rho \nu_t$ and takes into account the dynamic molecular (μ) and the turbulent viscosity effects ($\rho \nu_t$); ν_t (m^2/s) is the

eddy viscosity, which is provided by the turbulence closure model. Finally, the compression velocity u_{ci} (m/s) is calculated as $u_{ci} = \min[c_\alpha |u_i|, \max(|u_i|)] \frac{\frac{\partial \alpha}{\partial x_i}}{|\frac{\partial \alpha}{\partial x_i}|}$, where the compression coefficient c_α (-) is assumed to be 1 (Weller, 2008; Marschall et al., 2012).

The VARANS equations allow to model the flow inside an eventual porous material which is modelled as a continuous media. with additional terms considered in the momentum equation to account for frictional forces exerted by the porous media. The mass and the momentum conservation equations, coupled to the VOF equation, read as follows:

$$\frac{\partial}{\partial x_i}\frac{\bar{u}_i}{n} = 0 \tag{4}$$

$$\begin{aligned}(1+c)\frac{\partial}{\partial t}\frac{\rho \bar{u}_i}{n} + \frac{\bar{u}_j}{n}\frac{\partial}{\partial x_j}\frac{\rho \bar{u}_i}{n} = &- g_j x_j \frac{\partial \rho}{\partial x_i} - \frac{\partial \bar{p}^*}{\partial x_i} - f_{\sigma i} - \frac{\partial}{\partial x_j}\mu_{\text{eff}}\Big(\frac{\partial}{\partial x_j}\frac{\rho \bar{u}_i}{n} + \frac{\partial}{\partial x_i}\frac{\rho \bar{u}_i}{n}\Big) + \\ &- A\bar{u}_i - B|\bar{u}_i|\bar{u}_i\end{aligned} \tag{5}$$

$$\frac{\partial \alpha}{\partial t} + \frac{\partial}{\partial x_i}\frac{\bar{u}_i \alpha}{n} + \frac{\partial}{\partial x_i}\frac{\bar{u}_{ci}\alpha(1-\alpha)}{n} = 0 \tag{6}$$

where $\bar{u}_i$ (m/s) are the volume averaged ensemble averaged velocity (or Darcy velocity) components, defined as $\bar{u}_i = \frac{1}{V_f}\int_{V_f} u_i dV$, being V_f (m^3) the fluid volume contained in the averaging volume V, n (-) is the porosity, defined as the volume of voids over the total volume, and $\bar{p}^*$ (Pa) the volume averaged ensemble averaged pressure in excess of hydrostatic defined as $\bar{p}^* = \frac{1}{V_f}\int_{\partial V_f} p^* dS$ (see del Jesus et al., 2012). The coefficient A (-) takes into account the frictional force induced by laminar Darcy-type flow, B (-) accounts for the frictional force induced under turbulent flow conditions and c (-) considers the added mass. Following the work of Engelund (1953), modified by Van Gent (1995), the expressions for A, B and c are as follows:

$$A = a\frac{(1-n)^2}{n^3}\frac{\mu}{D_{50}^2}, \tag{7}$$

$$B = b\Big(1 + \frac{7.5}{KC}\Big)\frac{(1-n)}{n^3}\frac{\rho}{D_{50}}, \tag{8}$$

$$c = \gamma\frac{1-n}{n}, \tag{9}$$

where D_{50} (m) is the mean nominal diameter of the porous material, KC (-) the Keulegan-Carpenter number, a (-) and b (-) are empirical non-dimensional coefficients (see Lara et al., 2011; Losada et al., 2016) and $\gamma = 0.34$ (-) is a non dimensional parameter as proposed by Van Gent (1995).

These equations were first implemented in a solver within the OpenFOAM® framework by Higuera et al. (2014a,b) and later by Romano et al. (2020), to achieve a total mass conservation.. The solver works as follows: at the clear fluid region (i.e. outside the porous region) the frictional forces exerted by the porous media are deleted (i.e. $a = b = c = 0$) and $n = 1$, thus the VARANS are replaced by the RANS; inside the porous region the empirical coefficients, the parameters and the porosity related to the porous media (i.e. a, b, c, D_{50}, KC and n) are defined, thus the full set of VARANS is solved. More details on the VARANS equations can be found in del Jesus et al. (2012), Lara et al. (2012) and Losada et al. (2016), while for a more thorough description of their implementation in OpenFOAM® we refer to Romano et al. (2020). Finally, it should be mentioned that the solver supports several turbulence models (e.g. two equation models, k-ε, k-ω, and k-ω-SST). In this study, the k-ω-SST turbulence model has been used, with the enhancement from Larsen and Fuhrman (2018) to to deal with the overproduction of turbulence levels.

To simulate the behavior of the granular material (i.e., the deformable landslide) a Coulomb viscoplastic rheology (Non-Newtonian rheology) (Domnik and Pudasaini, 2012) has been implemented in the OpenFOAM® framework. It is important to highlight that this rheology has been

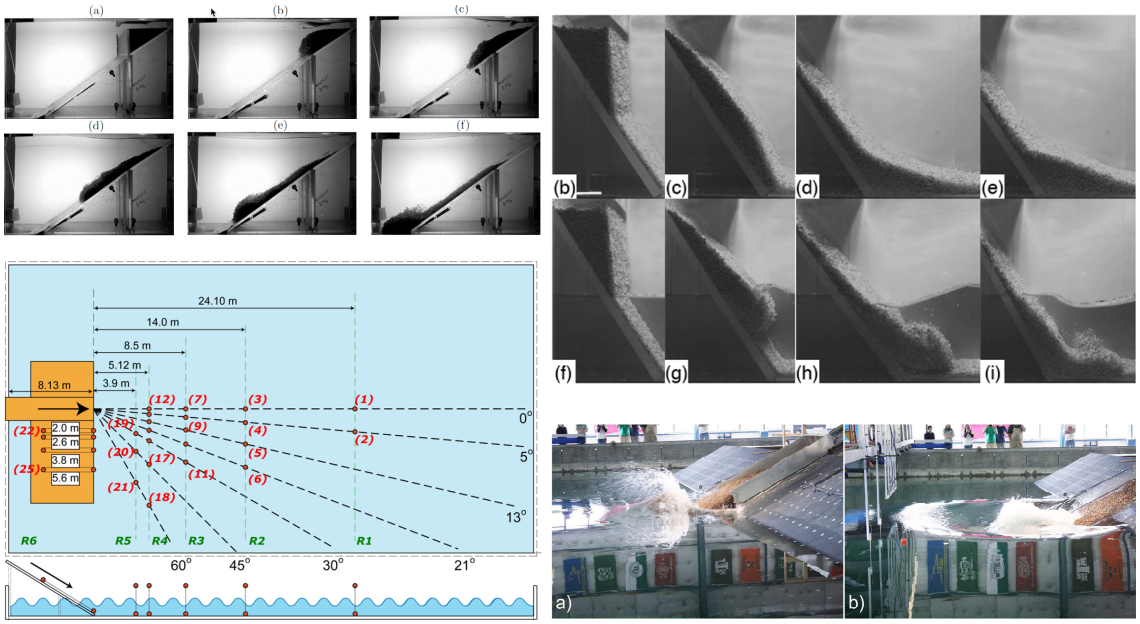

Figure 1: Pictures and experimental sketch of the three benchmark cases numerically reproduced. Note that pictures and sketch adapted from Grilli et al. (2017), Viroulet et al. (2014) and Mohammed and Fritz (2012).

originally implemented and validated in OpenFOAM® by von Boetticher et al. (2016) in the solver *interMixingFoam*. The reader is referred to Domnik and Pudasaini (2012) and von Boetticher et al. (2016) for further details related to theoretical aspects.

LANDSLIDE TSUNAMI BENCHMARKS

To test the capability of the numerical approach to reproduce tsunamis induced by granular landslides three experimental benchmark cases from the literature (`http://www1.udel.edu/kirby/landslide/problems.html` Kirby et al., 2022) has been numerically reproduced. The three benchmark cases have been selected with the aim of exploring a wide range of conditions and configurations for landslide-generated tsunamis. In fact, different initial landslide positions, spanning from submerged to subaerial landslides, and velocities, spanning from resting to accelerated landslides, have been chosen thus investigating and stressing the capability of the numerical model to reproduce different landslide contitions: I) a 2D case of submerged landslide Grilli et al. (2017); II) a 2D case of subaerial landslide Viroulet et al. (2014); III) a 3D case of subaerial landslide Mohammed and Fritz (2012).

$2D$ submerged landslide

Here a brief description of the 2D submerged case (Grilli et al., 2017) is given. These laboratory experiments of tsunami generated by underwater deformable landslides have been performed at the Ecole Centrale de Marseille (IRPHE, Marseille, France). The experimental setup is made up of a wave flume of length $l = 6.27$ m and width $w = 0.25$ m and a slope (slope angle $\theta = 35°$) was placed at one edge of the flume. The granular landslides are modelled by a volume of glass beads (density $\rho_b = 2500$ kg/m^3). In each experiment, a mass of beads was submerged in fresh water (density $\rho_w = 1000$ kg/m^3), in a reservoir of triangular shape located on the slope, fronted by a sluice gate.

The experiments consisted in instantaneously withdrawing the gate, thus the beads were released along the slope, generating the impulsive waves that propagate along the flume. During the experiments water depth ($h = 0.320$-0.370 m), beads diameter ($d_b = 4$ and 10 mm) and dry mass ($M_b = 1.5$-2.5 kg) have been varied. Pictures of the experiments are shown in the upper left panels of Figure 1. The Readers are referred to Grilli et al. (2017) for a more exhaustive description of

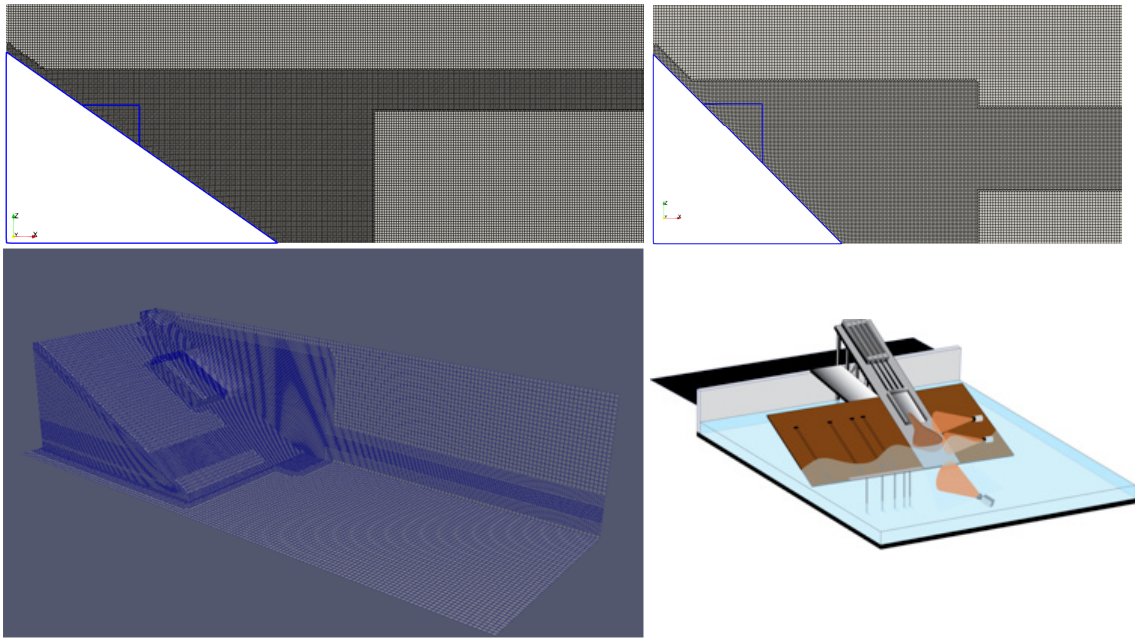

Figure 2: Example of the numerical mesh used to simulate the three benchmark cases. For all the numerical cases an extra refinement of the mesh is applied around the free surface, along the slope and at the toe of the slope. Lower right panel is adapted from Mohammed and Fritz (2012).

the benchmark.

$2D$ subaerial landslide

Here a brief description of the 2D subaerial case Viroulet et al. (2014) is given. These laboratory experiments of tsunami generated by subaerial deformable landslides have been performed at the Ecole Centrale de Marseille (IRPHE, Marseille, France). The experimental setup is made up of a wave flume of length $l = 2.20$ m and width $w = 0.20$ m and a slope (slope angle in the range $\theta = 35°$-$60°$) was placed at one edge of the flume. The granular landslides are modelled by a volume of glass beads (density $\rho_b = 2500$ kg/m^3) initially contained in a triangular cavity, placed above the still water level (water depth $h = 0.148$ m) and fronted by a sluice gate. In each experiment, a mass of beads was submerged in fresh water (density $\rho_w = 1000$ kg/m^3), in a reservoir of triangular shape located on the slope. Also in this case, the experiments consisted in instantaneously withdrawing the gate, thus the beads were released along the slope, generating the impulsive waves that propagate along the flume. Pictures of the experiments are shown in the upper right panels of Figure 1.

$3D$ subaerial landslide

Finally, here a brief description of the 3D subaerial case (Mohammed and Fritz, 2012) is given. These laboratory experiments of tsunami generated by subaerial deformable landslides have been performed at the tsunami wave basin (TWB) of the Network for Earthquake Engineering Simulation (NEES) at Oregon State University (Corvallis, Oregon, USA). The experimental setup is made up of a wave basin of length $l = 48.80$ m and width $w = 26.50$ m, with varying still water depths. A hillslope (slope angle $\theta = 27.1°$) was placed at the left hand side of the basin. A 9.3 m long steel plate was used as sliding surface. The granular landslides are modelled by a volume of naturally rounded river gravel (particle size in the range $d_g = 6.35$-19.05 mm, d50 = 13.7 mm; density $\rho_b = 2600$ kg/m^3) initially contained into a box (2.1 m $\times$ 1.2 m $\times$ 0.3 m), placed on the sliding surface, that can be accelerated by a pneumatic pistons system.

The experiments consisted in accelerating the box containing the landslide, thus the slide velocity corresponding to the box velocity. The landslide is released as the box reaches the maxi-

mum velocity. Then, the deformable granular landslide collapses down the hillslope while the box is decelerated and slides down simulating a gravity driven inertial granular landslide. During the experiments water depth (h = 0.3, 0.6, 0.9 and 1.2 m) and pressure in the pneumatic pistons (P = 145, 116, 87 and 58 psi), corresponding to different landslide velocities, have been varied. A sketch of the experimental setup is shown in the lower left panel of Figure 1, while some pictures of the experiments are shown in the lower right panels of the same figure. The Readers are referred to Mohammed and Fritz (2012) for a more exhaustive description of the benchmark.

The three benchmark cases have been numerically reproduced in OpenFOAM®. Two 2D numerical wave flumes have been created for reproducing the submerged (Grilli et al., 2017) and the subaerial (Viroulet et al., 2014) landslide cases (see upper panels of Figure 2), respectively, while a 3D numerical wave tank has been created for reproducing the experiment of Mohammed and Fritz (2012) (see lower panels of Figure 2). As can be seen in Figure 2, for all the numerical cases around the free surface, along the slope and at the toe of the slope (i.e., runout region) the mesh has been extra refined.

PRELIMINARY RESULTS

In this section some preliminary numerical results are provided and compared with the experimental ones. Figure 3 shows two selected snapshots of the interaction between the granular landslide and the water body for both the submerged 2D case (upper panel) and the subaerial 2D case (lower panel). The velocity magnitude pattern for water is represented in each panel by using color maps, while the gray filled area represents the slope and the yellow filled area represents the granular landslide. The two panels provide a first qualitative representation of the tsunami generation physics. In the upper panel (submerged landslide) it can be clearly seen that after the landslide triggering the granular material starts to deform, sliding along the slope, and a wave trough is generated on top of the lanslide, while a wave crest in front of the landslide itself is pushed by the moving landslide itself. On the contrary, looking at the lower panel of Figure 3, the impulsive wave generation due to a subaerial landslide is shown. In this case, it can be clearly seen the piston-like mechanisms induced by the landslide that pushes the water forming the first wave crest when entering the water.

A similar plot is presented in Figure 4, where six selected snapshots show the evolution in time of the interaction between the granular landslide and the water body for the subaerial 3D case (Mohammed and Fritz, 2012). The six panels depict the evolution in time of the interaction between the granular landslide and the water body magnifying the complex 3D phenomena that take place. The velocity magnitude pattern, both for landslide and water, is represented in each panel by using color maps. As represented in the figure, the landslide hits the water surface and enters the water, generating a wave crest, following the typical piston-like mechanism. Then, the generated wave propagate away from the generation are and the landslide reaches the bottom of the flume, arresting its motion. The figure clearly shows the runup pattern along the shoreline.

After these qualitative results, some preliminary quantitative results are presented. Figure 5 presents the comparison between experimental and numerical free surface elevation time series measured at the closest (considered from the landslide impact point) wave gauge for the three benchmark cases. The upper panel refers to the submerged 2D landslide (Grilli et al., 2017), while the middle panel refers to the subaerial 2D case (Viroulet et al., 2014), and finally the lower panel refers to the subaerial 3D case (Mohammed and Fritz, 2012). Note that for the 3D case the closest wave gauges is placed exactly in front of the generation area. In the figure, full black diamonds refer to experimental results, while thin red lines refer to numerical ones.

Overall a very good agreement between experimental and numerical results for the three benchmark cases, especially referring to the first three wave crests and troughs. We can notice that for the submerged 2D case and for the suabaerial 3D case small discrepancies between numerical and experimental results can be seen in the tralinig waves. This aspect can be possibly possibly related to the not perfect reproduction of the final part of the landslide evolution for the 2D case and to the possible difference of the initial conditions for the 3D case (i.e., landslide material accelerated during the experiments). Moreover, looking at the subaerial 2D case a slight overestimation of the first wave crest can be noticed. Nevertheless, overall a very good agreement between experimental

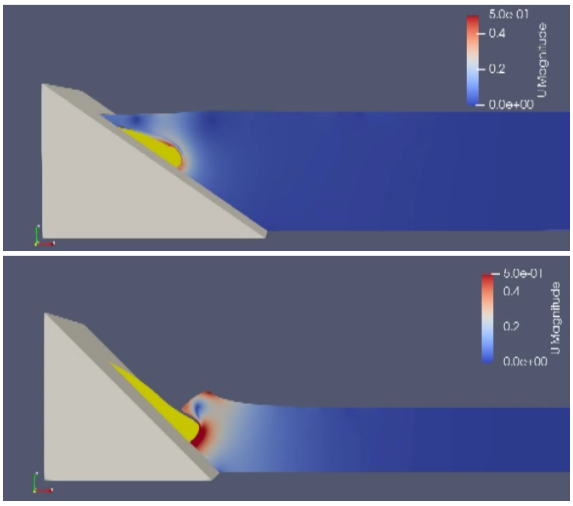

Figure 3: Snapshots of the interaction between the granular landslide and the water body for both the submerged 2D case (upper panel) and the subaerial 2D case (lower panel). The velocity magnitude pattern for water is represented in each panel by using color maps, while the gray filled area represents the slope.

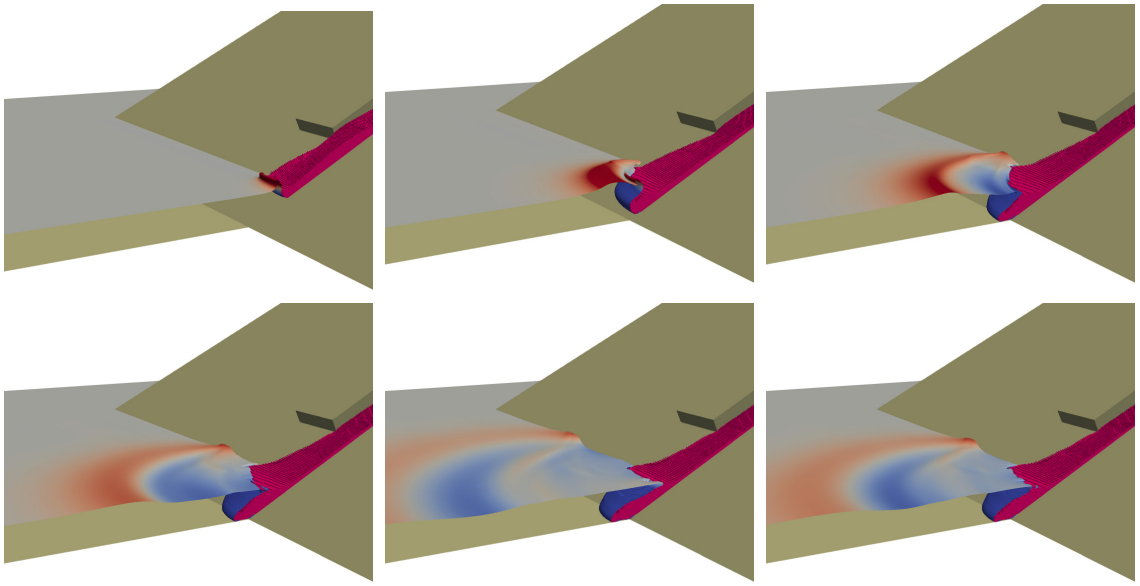

Figure 4: Six snapshots of the interaction between the granular landslide and the water body for both the submerged 3D case. The velocity magnitude pattern is represented in each panel by using color maps.

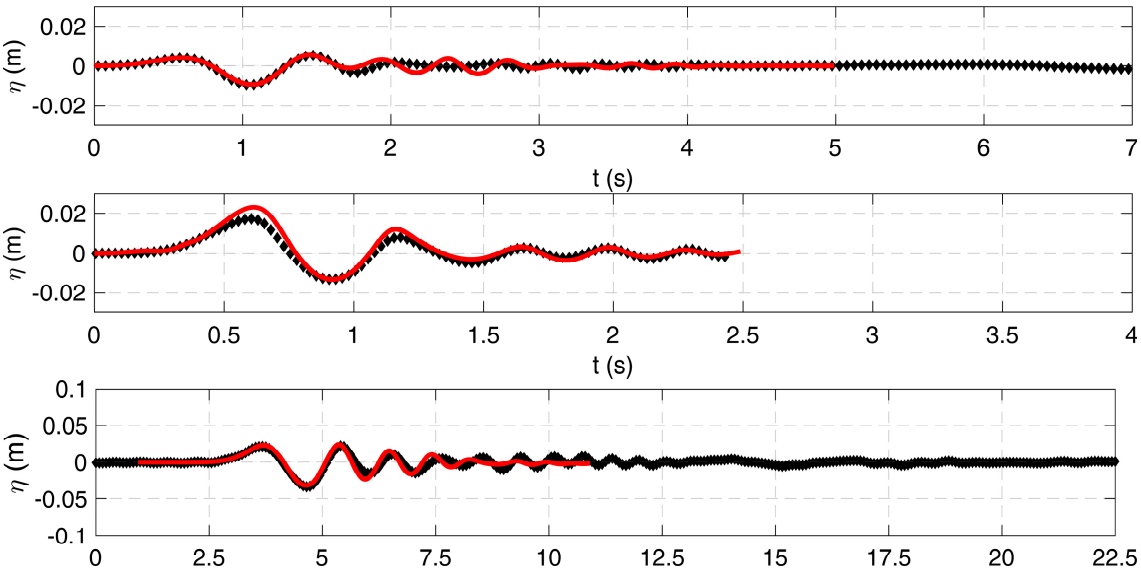

Figure 5: Comparison between experimental and numerical free surface elevation time series measured at the closest (considered from the landslide impact point) wave gauge for the three benchmark cases: submerged 2D landslide (upper panel), subaerial 2D case (middle panel), subaerial 3D case (lower panel). Full black diamonds refer to experimental results, while thin red lines refer to numerical ones.

and numerical results, especially referring to the first three wave crests and troughs, is obtained at the closest wave gauges for the three experimental benchmarks.

CONCLUDING REMARKS AND FUTURE WORKS

In this paper, the preliminary modelling results of tsunamis generated by deformable landslides in OpenFOAM® have been presented. Within this numerical framework the granular material (i.e., the landslide) is modelled by using a Coulomb viscoplastic rheology (Non-Newtonian rheology, von Boetticher et al., 2016; Domnik and Pudasaini, 2012) implemented in *multiPhaseInterFoam*. This numerical framework has been applied to reproduce three literature benchmark cases identified by tsunamis experts: I) a 2D submerged landslide case Grilli et al. (2017); II) a 2D subaerial landslide case Viroulet et al. (2014); III) and 3D subaerial landslide case Mohammed and Fritz (2012).

Qualitative and quantitative preliminary results have been presented. Specifically, the comparison between experimental and numerical free surface elevation time series measured at the closest (considered from the landslide impact point) wave gauge for the three benchmark cases has been presented showing an overall very good agreement between experimental and numerical results.

A more detailed comparison between experimental and numerical results should be carried out in the future, comparing not only free surface elevation at the closest wave gauges but also landslide evolution in space, free surface elevation time series at different wave gauges and runup time series (for the 3D case).

ACKNOWLEDGEMENTS

The authors acknowledge the financial support from the Government of Cantabria through the Fénix Program. The kind help of Prof. Hermann Fritz, which provided further information on the 3D subaerial case, is warmly acknowledged.

References

S. Abadie, D. Morichon, S. Grilli, and S. Glockner. Numerical simulation of waves generated by landslides using a multiple-fluid Navier–Stokes model. *Coastal Engineering*, 57(9):779–794, 2010.

S. Abadie, J. Harris, S. Grilli, and R. Fabre. Numerical modeling of tsunami waves generated by the flank collapse of the Cumbre Vieja Volcano (La Palma, Canary Islands): tsunami source and near field effects. *Journal of Geophysical Research: Oceans*, 117(C5), 2012.

S. Abadie, A. Paris, R. Ata, S. Le Roy, G. Arnaud, A. Poupardin, L. Clous, P. Heinrich, J. Harris, R. Pedreros, et al. La palma landslide tsunami: computation of the tsunami source with a calibrated multi-fluid navier-stokes model and wave impact assessment with propagation models of different types. *Natural Hazards and Earth System Sciences Discussions*, pages 1–50, 2019.

G. Bellotti and A. Romano. Wavenumber-frequency analysis of landslide-generated tsunamis at a conical island. Part II: EOF and modal analysis. *Coastal Engineering*, 128:84–91, 2017.

G. Bellotti, C. Cecioni, and P. De Girolamo. Simulation of small-amplitude frequency-dispersive transient waves by means of the mild-slope equation. *Coastal Engineering*, 55(6):447–458, 2008.

J. U. Brackbill, D. B. Kothe, and C. Zemach. A continuum method for modeling surface tension. *Journal of Computational Physics*, 100(2):335–354, 1992.

C. Cecioni, A. Romano, G. Bellotti, M. Di Risio, and P. De Girolamo. Real-time inversion of tsunamis generated by landslides. *Natural Hazards & Earth System Sciences*, 11(9), 2011.

F. Chen, V. Heller, and R. Briganti. Numerical modelling of tsunamis generated by iceberg calving validated with large-scale laboratory experiments. *Advances in Water Resources*, 142:103647, 2020. ISSN 0309-1708.

L. Clous and S. Abadie. Simulation of energy transfers in waves generated by granular slides. *Landslides*, pages 1–17, 2019.

P. De Girolamo, M. Di Risio, A. Romano, and M. Molfetta. Landslide tsunami: physical modeling for the implementation of tsunami early warning systems in the mediterranean sea. *Procedia Engineering*, 70:429–438, 2014.

M. del Jesus, J. L. Lara, and I. J. Losada. Three-dimensional interaction of waves and porous coastal structures: Part I: Numerical model formulation. *Coastal Engineering*, 64:57–72, 2012.

M. Di Risio, G. Bellotti, A. Panizzo, and P. De Girolamo. Three-dimensional experiments on landslide generated waves at a sloping coast. *Coastal Engineering*, 56(5-6):659–671, MAY-JUN 2009a. ISSN 0378-3839. doi: {10.1016/j.coastaleng.2009.01.009}.

M. Di Risio, P. De Girolamo, G. Bellotti, A. Panizzo, F. Aristodemo, M. G. Molfetta, and A. F. Petrillo. Landslide-generated tsunamis runup at the coast of a conical island: New physical model experiments. *Journal of Geophysical Research-Oceans*, 114, JAN 20 2009b. ISSN 0148-0227. doi: {10.1029/2008JC004858}.

B. Domnik and S. P. Pudasaini. Full two-dimensional rapid chute flows of simple viscoplastic granular materials with a pressure-dependent dynamic slip-velocity and their numerical simulations. *Journal of Non-Newtonian Fluid Mechanics*, 173:72–86, 2012.

F. Enet and S. T. Grilli. Experimental study of tsunami generation by three-dimensional rigid underwater landslides. *Journal Of Waterway Port Coastal And Ocean Engineering-ASCE*, 133 (6):442–454, NOV-DEC 2007. ISSN 0733-950X. doi: 10.1061/(ASCE)0733-950X(2007)133: 6(442).

F. Engelund. On the laminar and turbulent flows of ground water through homogeneous sand. *Transactions of the Danish: Academy of Technical Sciences*, (3):356–361, 1953.

A. Franci, M. Cremonesi, U. Perego, G. Crosta, and E. Oñate. 3d simulation of vajont disaster. part 1: Numerical formulation and validation. *Engineering Geology*, 279:105854, 2020.

H. M. Fritz, F. Mohammed, and J. Yoo. Lituya Bay landslide impact generated mega-tsunami 50th anniversary. *Pure and Applied Geophysics*, 166(1-2):153–175, 2009.

S. T. Grilli, O.-D. S. Taylor, C. D. Baxter, and S. Maretzki. A probabilistic approach for determining submarine landslide tsunami hazard along the upper east coast of the united states. *Marine Geology*, 264(1-2):74–97, 2009.

S. T. Grilli, M. Shelby, O. Kimmoun, G. Dupont, D. Nicolsky, G. Ma, J. T. Kirby, and F. Shi. Modeling coastal tsunami hazard from submarine mass failures: effect of slide rheology, experimental validation, and case studies off the us east coast. *Natural Hazards*, 86(1):353–391, 2017.

S. T. Grilli, D. R. Tappin, S. Carey, S. F. Watt, S. N. Ward, A. R. Grilli, S. L. Engwell, C. Zhang, J. T. Kirby, L. Schambach, and M. Muslim. Modelling of the tsunami from the December 22, 2018 lateral collapse of Anak Krakatau volcano in the Sunda Straits, Indonesia. *Scientific Reports*, 9, 2019.

V. Heller and W. H. Hager. Impulse product parameter in landslide generated impulse waves. *Journal of Waterway, Port, Coastal, and Ocean Engineering*, 136(3):145–155, 2010.

V. Heller and J. Spinneken. On the effect of the water body geometry on landslide–tsunamis: Physical insight from laboratory tests and 2D to 3D wave parameter transformation. *Coast. Eng.*, 104:113–134, 2015.

V. Heller, M. Bruggemann, J. Spinneken, and B. D. Rogers. Composite modelling of subaerial landslide–tsunamis in different water body geometries and novel insight into slide and wave kinematics. *Coastal Engineering*, 109:20–41, 2016.

P. Higuera, J. L. Lara, and I. J. Losada. Realistic wave generation and active wave absorption for Navier–Stokes models: Application to OpenFOAM®. *Coastal Engineering*, 71:102–118, 2013a.

P. Higuera, J. L. Lara, and I. J. Losada. Simulating coastal engineering processes with OpenFOAM®. *Coastal Engineering*, 71:119–134, 2013b.

P. Higuera, J. L. Lara, and I. J. Losada. Three-dimensional interaction of waves and porous coastal structures using OpenFOAM®. Part I: formulation and validation. *Coastal Engineering*, 83:243–258, 2014a.

P. Higuera, J. L. Lara, and I. J. Losada. Three-dimensional interaction of waves and porous coastal structures using OpenFOAM®. Part II: Application. *Coastal Engineering*, 83:259–270, 2014b.

H. Jasak. Error analysis and estimation for the finite volume method with applications to fluid flows. *(Ph.D thesis) Imperial College London (University of London)*, 1996.

G.-B. Kim, W. Cheng, R. C. Sunny, J. J. Horrillo, B. C. McFall, F. Mohammed, H. M. Fritz, J. Beget, and Z. Kowalik. Three dimensional landslide generated tsunamis: Numerical and physical model comparisons. *Landslides*, pages 1–17, 2019a.

J. Kim, F. Løvholt, D. Issler, and C. F. Forsberg. Landslide material control on tsunami genesisâ€"the Storegga slide and tsunami (8,100 years bp). *Journal of Geophysical Research: Oceans*, 2019b.

J. T. Kirby, S. T. Grilli, J. Horrillo, P. L.-F. Liu, D. Nicolsky, S. Abadie, B. Ataie-Ashtiani, M. J. Castro, L. Clous, C. Escalante, et al. Validation and inter-comparison of models for landslide tsunami generation. *Ocean Modelling*, 170:101943, 2022.

J. L. Lara, I. J. Losada, M. Maza, and R. Guanche. Breaking solitary wave evolution over a porous underwater step. *Coastal Engineering*, 58(9):837–850, 2011.

J. L. Lara, M. del Jesus, and I. J. Losada. Three-dimensional interaction of waves and porous coastal structures: Part II: Experimental validation. *Coastal Engineering*, 64:26–46, 2012.

B. E. Larsen and D. R. Fuhrman. On the over-production of turbulence beneath surface waves in reynolds-averaged navier–stokes models. *Journal of Fluid Mechanics*, 853:419–460, 2018.

C.-H. Lee and Z. Huang. Effects of grain size on subaerial granular landslides and resulting impulse waves: experiment and multi-phase flow simulation. *Landslides*, 19(1):137–153, 2022.

E. K. Lindstrøm. Waves generated by subaerial slides with various porosities. *Coastal Engineering*, 116:170–179, 2016.

P.-F. Liu, T.-R. Wu, F. Raichlen, C. Synolakis, and J. Borrero. Runup and rundown generated by three-dimensional sliding masses. *Journal of Fluid Mechanics*, 536:107–144, 2005.

I. J. Losada, J. L. Lara, and M. del Jesus. Modeling the interaction of water waves with porous coastal structures. *Journal of Waterway, Port, Coastal, and Ocean Engineering*, 142 (6):03116003, 2016. doi: 10.1061/(ASCE)WW.1943-5460.0000361.

F. Løvholt, C. B. Harbitz, and K. B. Haugen. A parametric study of tsunamis generated by submarine slides in the Ormen Lange/Storegga area off western Norway. In *Ormen Lange–an Integrated Study for Safe Field Development in the Storegga Submarine Area*, pages 219–231. Elsevier, 2005.

F. Løvholt, G. Pedersen, C. B. Harbitz, S. Glimsdal, and J. Kim. On the characteristics of landslide tsunamis. *Philosophical Transactions of the Royal Society A: Mathematical, Physical and Engineering Sciences*, 373(2053):20140376, 2015.

P. Lynett and P. L. F. Liu. A numerical study of the run-up generated by three-dimensional landslides. *Journal of Geophysical Research-Oceans*, 110(C3), MAR 8 2005. ISSN 0148-0227. doi: {10.1029/2004JC002443}.

G. Ma, J. T. Kirby, T.-J. Hsu, and F. Shi. A two-layer granular landslide model for tsunami wave generation: Theory and computation. *Ocean Modelling*, 93:40–55, 2015.

H. Marschall, K. Hinterberger, C. Schüler, F. Habla, and O. Hinrichsen. Numerical simulation of species transfer across fluid interfaces in free-surface flows using OpenFOAM. *Chemical Engineering Science*, 78:111–127, 2012.

B. C. McFall and H. M. Fritz. Physical modelling of tsunamis generated by three-dimensional deformable granular landslides on planar and conical island slopes. *Proceedings of the Royal Society of London. Series A: Mathematical, Physical and Engineering Sciences*, 472–2188:20160052, 2016.

F. Mohammed and H. M. Fritz. Physical modeling of tsunamis generated by three-dimensional deformable granular landslides. *Journal of Geophysical Research: Oceans (1978–2012)*, 117 (C11), 2012.

F. Montagna, G. Bellotti, and M. Di Risio. 3D numerical modeling of landslide-generated tsunamis around a conical island. *Natural Hazards*, 58(1):591–608, 2011.

R. P. Mulligan, A. Franci, M. A. Celigueta, and W. A. Take. Simulations of landslide wave generation and propagation using the particle finite element method. *Journal of Geophysical Research: Oceans*, 125(6):e2019JC015873, 2020. doi: 10.1029/2019JC015873.

A. Panizzo, P. De Girolamo, M. Di Risio, A. Maistri, and A. Petaccia. Great landslide events in italian artificial reservoirs. *Natural Hazards and Earth System Sciences*, 5(5):733–740, 2005. doi: 10.5194/nhess-5-733-2005.

A. Paris, P. Heinrich, and S. Abadie. Landslide tsunamis: Comparison between depth-averaged and navier-stokes models. *Coastal Engineering*, 170:104022, 2021. ISSN 0378-3839. doi: https://doi.org/10.1016/j.coastaleng.2021.104022. URL `https://www.sciencedirect.com/science/article/pii/S0378383921001678`.

M. Rauter, L. Hoße, R. Mulligan, W. Take, and F. Løvholt. Numerical simulation of impulse wave generation by idealized landslides with openfoam. *Coastal Engineering*, 165:103815, 2021. ISSN 0378-3839.

M. Rauter, S. Viroulet, S. S. Gylfadóttir, W. Fellin, and F. Løvholt. Granular porous landslide tsunami modelling–the 2014 lake askja flank collapse. *Nature communications*, 13(1):1–13, 2022.

A. Romano, G. Bellotti, and M. Di Risio. Wavenumber–frequency analysis of the landslide-generated tsunamis at a conical island. *Coastal Engineering*, 81:32–43, 2013.

A. Romano, M. Di Risio, G. Bellotti, M. Molfetta, L. Damiani, and P. De Girolamo. Tsunamis generated by landslides at the coast of conical islands: experimental benchmark dataset for mathematical model validation. *Landslides*, 13(6):1379–1393, 2016.

A. Romano, M. Di Risio, M. G. Molfetta, G. Bellotti, D. Pasquali, P. Sammarco, L. Damiani, and P. De Girolamo. 3D physical modeling of tsunamis generated by submerged landslides at a conical island: The role of initial acceleration. *Coastal Engineering Proceedings*, 1(35):14, 2017.

A. Romano, J. L. Lara, G. Barajas, B. Di Paolo, G. Bellotti, M. Di Risio, I. J. Losada, and P. De Girolamo. Tsunamis generated by submerged landslides: Numerical analysis of the near-field wave characteristics. *Journal of Geophysical Research: Oceans*, 125(7):e2020JC016157, 2020.

G. Ruffini, V. Heller, and R. Briganti. Numerical modelling of landslide-tsunami propagation in a wide range of idealised water body geometries. *Coastal Engineering*, page 103518, 2019.

C. Shi, Y. An, Q. Wu, Q. Liu, and Z. Cao. Numerical simulation of landslide-generated waves using a soil–water coupling smoothed particle hydrodynamics model. *Advances in Water Resources*, 92:130–141, 2016.

P. Si, H. Shi, and X. Yu. A general numerical model for surface waves generated by granular material intruding into a water body. *Coastal Engineering*, 142:42–51, 2018.

T. Takabatake, D. C. Han, J. J. Valdez, N. Inagaki, M. Mäll, M. Esteban, and T. Shibayama. Three-dimensional physical modeling of tsunamis generated by partially submerged landslides. *Journal of Geophysical Research: Oceans*, 127(1):e2021JC017826, 2022.

M. R. A. Van Gent. Wave interaction with permeable coastal structures. *(Ph.D thesis) Delft University*, 1995.

S. Viroulet, A. Sauret, and O. Kimmoun. Tsunami generated by a granular collapse down a rough inclined plane. *EPL (Europhysics Letters)*, 105(3):34004, 2014.

A. von Boetticher, J. M. Turowski, B. W. McArdell, D. Rickenmann, and J. W. Kirchner. Debrisintermixing-2.3: a finite volume solver for three-dimensional debris-flow simulations with two calibration parameters–part 1: Model description. *Geoscientific Model Development*, 9(9): 2909–2923, 2016.

P. Watts. Wavemaker curves for tsunamis generated by underwater landslides. *Journal of Waterway, Port, Coastal, and Ocean Engineering*, 124(3):127–137, 1998. doi: 10.1061/(ASCE) 0733-950X(1998)124:3(127).

P. Watts, S. Grilli, J. Kirby, G. Fryer, and D. Tappin. Landslide tsunami case studies using a Boussinesq model and a fully nonlinear tsunami generation model. *Natural Hazards And Earth System Sciences*, 3(5):391–402, 2003.

H. G. Weller. A new approach to vof-based interface capturing methods for incompressible and compressible flow. *OpenCFD Ltd., Report TR/HGW*, 4, 2008.

C. Whittaker, R. Nokes, H.-Y. Lo, P.-F. Liu, and M. Davidson. Physical and numerical modelling of tsunami generation by a moving obstacle at the bottom boundary. *Environmental Fluid Mechanics*, 17(5):929–958, 2017.

G. Zitti, C. Ancey, M. Postacchini, and M. Brocchini. Impulse waves generated by snow avalanches: momentum and energy transfer to a water body. *Journal of Geophysical Research: Earth Surface*, 121(12):2399–2423, 2016.